IOP Conf. Series: Materials Science and Engineering **304** (2018) 012007 doi:10.1088/1757-899X/304/1/012007

Focussed ion beam thin sample microanalysis using a field emission gun electron probe microanalyser

Y Kubo

Sumitomo Electric Industries, Ltd., Analysis Technology Research Center, 1-1-3, Shimaya, Konohana-ku Osaka-shi, 554-0024 Osaka, Japan

E-mail: kubo-yugo@sei.co.jp; ykubo2733@gmail.com

Abstract. Field emission gun electron probe microanalysis (FEG-EPMA) in conjunction with wavelength-dispersive X-ray spectrometry using a low acceleration voltage (V_{acc}) allows elemental analysis with sub-micrometre lateral spatial resolution (SR). However, this degree of SR does not necessarily meet the requirements associated with increasingly miniaturised devices. Another challenge related to performing FEG-EPMA with a low V_{acc} is that the accuracy of quantitative analyses is adversely affected, primarily because low energy X-ray lines such as the L- and M-lines must be employed and due to the potential of line interference. One promising means of obtaining high SR with FEG-EPMA is to use thin samples together with high V_{acc} values. This mini-review covers the basic principles of thin-sample FEG-EPMA and describes an application of this technique to the analysis of optical fibres. Outstanding issues related to this technique that must be addressed are also discussed, which include the potential for electron beam damage during analysis of insulating materials and the development of methods to use thin samples for quantitative analysis.

1. Introduction

In the last decade, field emission gun electron probe microanalysis (FEG-EPMA) has been rapidly adopted by laboratories worldwide [1]. An FEG provides superior spatial resolution (SR) for X-ray imaging compared with conventional W- or LaB_6-units because it allows for a smaller electron beam spot size, even if a low acceleration voltage (V_{acc}) is used [1-7]. In this review, the SR is defined as the lateral width of the X-ray generation region. However, the SR obtained when using a FEG-EPMA under typical measurement conditions (meaning the V_{acc} and probe current (I_{prob})) applied in an actual laboratory is typically in the range of approximately 150 to 200 nm [4]. This does not necessarily meet the recent demands for materials design in various fields of engineering, in which the sizes of internal structures of devices are being increasingly reduced. A related topic is the Er-doped optical fibre amplifier (EDF) [8]. As shown in figures 1a and 1b, an EDF generally consists of a core composed of SiO_2 glass doped with impurities surrounded by a cladding of pure SiO_2 glass [8]. The refractive index of the core relative to that of the cladding is increased by doping with Ge at a level of approximately 1 - 5 % (by mass), to confine the optical signals to the core (figure 1a). Approximately 1 - 5 % (by mass) Al is also added to the core to assist in controlling the deviation in refractive gain, one of most important product characteristics [8]. Figures 1c-e show backscattered electron (BSE) images of the EDF cross-section ((c: perspective, (d: around the core, and (e: around the centre of the core). The core is the bright circular area with a diameter of about 2 μm in figure 1d. A local dark

area with a diameter of 100 nm is observed in the centre of the core (figure 1e), which indicates the fine distribution of the dopants. Analysis of the Al and Ge levels in these cores requires a minimum detection limit (MDL) of less than 5,000 ppm in conjunction with an SR below 50 nm. In addition to the aforementioned insufficient SR, another challenge associated with FEG-EPMA is the low V_{acc} values that are often employed, which can adversely affect the accuracy of quantitative analyses [9]. When operating FEG-EPMA instrumentation at a low V_{acc}, it is typical to use low-energy X-ray lines such as the L- and M-lines. However, these lines are often affected by spectroscopic effects such as peak shifts and overlaps [9]. The fluorescence yields for the L- and M-lines are also lower than that for conventional K-lines [9].

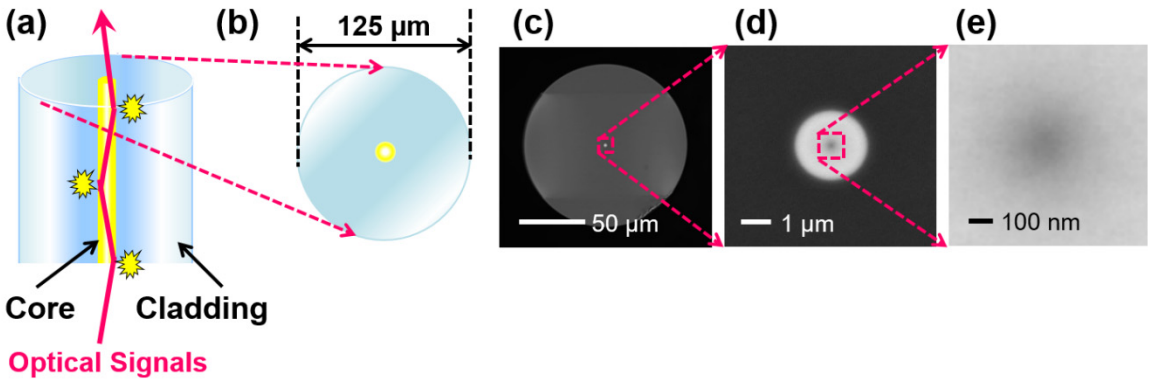

Figure 1. Diagrams of an EDF consisting of a core (SiO_2 glass doped with some impurities) surrounded by a cladding (pure SiO_2 glass). a) Side view, and b) cross-section. BSE images of an EDF cross-section showing c) the entire section, d) the region around the core, and e) the centre of the core. (Modified with permission from Ref. [14], copyright © Microscopy Society of America 2015.)

One approach to achieve a high SR while employing low energy X-rays is to thin the sample and also apply a high V_{acc} [10-14]. Figure 2 presents a schematic diagram showing SR improvement by sample thinning. As shown in the left diagram, the SR obtainable with conventional FEG-EPMA is poor when analysing bulk samples, since the area within which X-rays are generated is overly large. The SR is at best 150 - 200 nm under these conditions, even when using a low V_{acc} [4]. Thinned samples will increase the MDL because the characteristic X-ray intensity decreases as the sample is made thinner. Therefore, it is necessary to optimise both the measurement conditions and the sample thickness so as to balance the SR and MDL.

The general approach to the production of thin samples for electron beam microanalysis using energy-dispersive X-ray spectrometry (EDS) or wavelength-dispersive X-ray spectrometry (WDS) microanalysis, and the inherent advantages of this process with regard to data quantification have been known for quite some time. The basic concept appears to have been first suggested by Cliff and Lorimer's group in the 1970s [10, 15]. Subsequently, Joy *et al*. investigated the minimum detectable mass and minimum mass fraction for thin-sample X-ray analysis [16]. In the 1980s, Horita *et al*. proposed a method that does not require the sample thickness to be known for X-ray absorption corrections to be applied [17]. In addition, Watanabe's group reported the determination of the minimum detectable mass for electron-beam based EDS of thin samples at high acceleration voltages [18]. Thus, we consider that sample thinning will offer greater improvements in conjunction with FEG-EPMA than with conventional EPMA because the diameter of the electron beam can be made very small in the case of the former technique. Despite this, sample thinning as a preparation for FEG-EPMA has seldom been employed. This may be partly the result of the generally accepted view

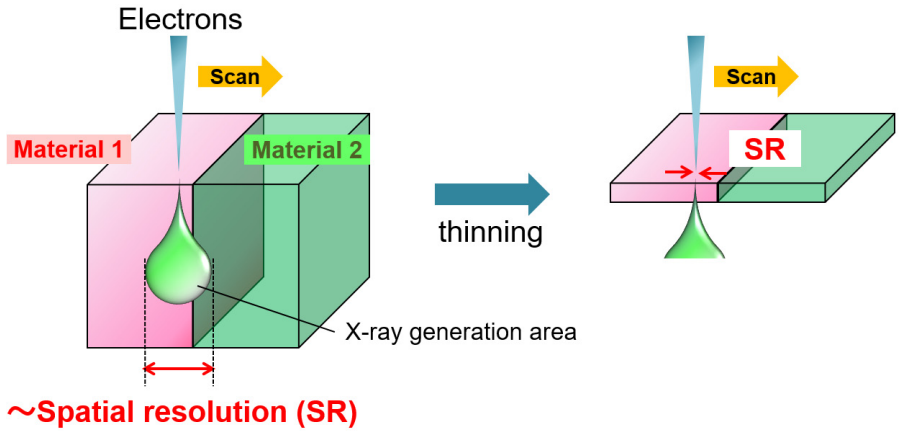

Figure 2. Schematic diagram of SR improvement by sample thinning. (Modified with permission from Ref. [13], copyright © 2015 Elsevier B.V. All rights reserved.)

that sample thinning significantly reduces the characteristic X-ray signals and, therefore, degrades the detection sensitivity. However, to the best of our knowledge, there have been no systematic investigations of the SR and MDL values associated with thin-sample FEG-EPMA. To address this issue, our own research group has been conducting studies related to thin-sample FEG-EPMA [12-14]. The purposes of this mini-review are to present a detailed examination of the potential SR and MDL values that can be obtained using this technique, to describe an example application to the analysis of an EDF, and to discuss remaining challenges. The present review also provides SR and MDL values determined for bulk samples when using FEG-EPMA and for thin samples via scanning transmission electron microscopy in conjunction with EDS (STEM-EDS). The latter technique is considered as an example of a more conventional microanalytical technique. In the work presented herein, sample thinning was performed using a Ga focussed ion beam (Ga-FIB) because this method allowed the fabrication of test specimens with positional accuracy on the nanometre scale. This technique was therefore well-suited to analysis of the EDF core at the centre of the optical fibre cross-section. The combination of Ga-FIB and EPMA has been previously demonstrated by Richter *et al*. [19-21]. They described a depth profile analysis of the structure of a multilayer system consisting of Al/SiO_2/GeSbTe on a SiO_2 substrate, during which they performed a line scan of a sample cross-section at an oblique angle prepared by FIB [19]. In another study [20], a similar technique was employed to examine the interfacial reactions within a multilayered NiAl-Hf-hBN system on a sapphire fibre. More recently, this same group described further improvement of the proposed bevel method by reducing the level of FIB artefacts and using microprobes with enhanced focussing optics [21].

2. Experimental methods

2.1. Sample preparation

InGaP films were grown on GaAs substrates using metal-organic vapour phase epitaxy. These InGaP/GaAs samples were subsequently thinned perpendicular to the layer structure, as shown in figure 2. STEM images confirmed that atomic diffusion across the InGaP/GaAs interface occurred over a distance of only several nanometres, and therefore these samples were suitable for evaluation of the SR.

2.2. Ga-FIB

The samples were thinned using Ga-FIB to thicknesses (T) of approximately 100, 130, 210, 310, and 430 nm, as confirmed by secondary electron images of the cross-sections [12, 13]. The sample mounting method has been described in detail in our previous report [12]. The cleaved cross-section of a bulk InGaP/GaAs sample was also analysed as a reference.

2.3. FEG-EPMA

X-ray line profiles and energy scans were obtained using an FEG-EPMA instrument (JEOL JXA-8530F). In each measurement, the working distance was approximately 11 mm, the take-off angle was 40° and In-Lα X-rays (critical excitation voltage: 3.73 keV) were employed. The radius of the Rowland circle was 100 mm (an H-type spectrometer with a JEOL microprobe) and the analysing crystal was made of pentaerythritol (PETH). The X-rays were collimated through a 0.5 mm wide slit and then detected using a sealed proportional counter filled with xenon. The measurement conditions included a probe current (I_{prob}) in the range of 5 - 200 nA, V_{acc} values of 30 kV (for thin samples), 5.5 or 10 kV (bulk samples), and a sampling time of 1 s per point. The electron beam was focussed. To assess the SR that could be obtained during FEG-EPMA, an In-Lα line profile was measured across the InGaP/GaAs interface. The electron beam was perpendicular to the plane of the thin samples and the line scan direction was perpendicular to the interface (figure 2). It should also be noted that the scan direction was set parallel to the PETH analysing crystal for all line scans so as to exclude X-ray defocusing effects.

2.4. STEM-EDS

In Lα X-ray line profiles across the InGaP/GaAs samples were acquired using a Si (Li) solid state detector (Genesis, EDAX) in conjunction with STEM (Hitachi, HD-2700). The sample was situated 2.43 mm below the objective lens and a take-off angle of 25.7° was employed. The distance between the sample and detector was 9.08 mm and the solid angle was 0.31 sr. The measurement conditions applied during STEM-EDS included an I_{prob} of 0.2 nA, a V_{acc} of 200 kV, a sampling time of 1 s per point, and a beam size of approximately 0.2 nm.

2.5. Evaluation of the SR

The SR values obtained with FEG-EPMA and STEM-EDS were defined as the distance over which the intensity of the In-Lα signal dropped from 84 % to 16 % of the difference between the average value in the InGaP layer and that in the GaAs substrate (figure 3a) [3, 22].

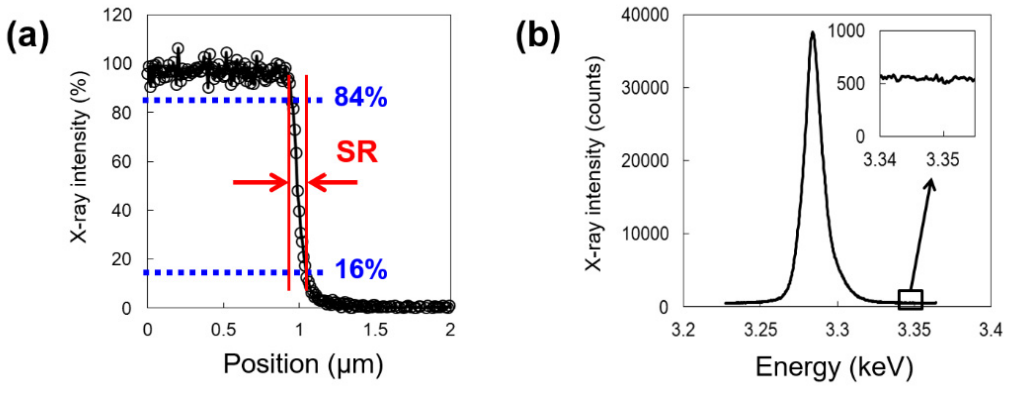

Figure 3. a) SR evaluated as the distance over which the intensity of the In-Lα signal drops from 84 % to 16 % of the difference between the average value in the InGaP layer and in the GaAs substrate. b) Energy scan of the In-Lα X-ray intensity for the InGaP layer. To evaluate the MDL values for thin-sample FEG-EPMA, the standard deviation (inset) in the area associated with the peak was calculated. (Modified with permission from Ref. [13], copyright © 2015 Elsevier B.V. All rights reserved.)

2.6. Evaluation of the MDL

The MDL values obtained from FEG-EPMA and STEM-EDS of In were evaluated based on the results obtained from energy scans of the InGaP layer using In-Lα X-rays. Firstly, the standard deviation *S*, for the background count associated with the peak [23] was calculated as depicted in figure 3b using the equation:

$$S = \left(\sum \frac{(Yi - Yave)^2}{n}\right)^{0.5}, \quad (1)$$

where *Y* is the X-ray signal at a given energy position in the energy scan and n is the number of data points. The *S*-values were converted from X-ray intensity (in counts) to concentration (in ppm (by mass)), where the conversion factor was determined as the ratio of the In-Lα peak intensity to the In concentration (known), assuming a linear relationship between the X-ray intensity and concentration. The MDL was then defined as equal to 3*S* (in ppm (by mass)). In the case of STEM-EDS, the background derived from continuous X-rays was subtracted prior to calculating *S*.

In addition, an EDF preform was prepared by conventional chemical vapour deposition [24] and formed into fibres that were subsequently used for SiO_2-based fibre fabrication. The EDF was cleaved and a flat, smooth cross-section was confirmed using an optical microscope. Thinning of the EDF sample was performed using Ga-FIB (Hitachi, FB2100) to a *T* of approximately 200 nm. The details of this preparation process have been fully described in our previous report [14].

3. Results and discussion

3.1. Variation of SR with V_{acc} in thin and bulk FEG-EPMA

Figures 4a and 4b show the In-Lα line profiles obtained from bulk and thin (*T* = 100 nm) InGaP/GaAs samples, respectively, at V_{acc} = 5.5, 10, 15, 20, 25, and 30 kV, and at an I_{prob} of 50 nA. Figure 4a indicates that the change in the In-Lα intensity across the InGaP/GaAs interface in the bulk sample is more gradual at higher V_{acc}. In contrast, the intensity change is sharper at higher V_{acc} in the case of the thin sample, as shown in figure 4b. Furthermore, at V_{acc} = 5.5 kV, the sharpness of the intensity change for the bulk sample is similar to that for the thin sample.

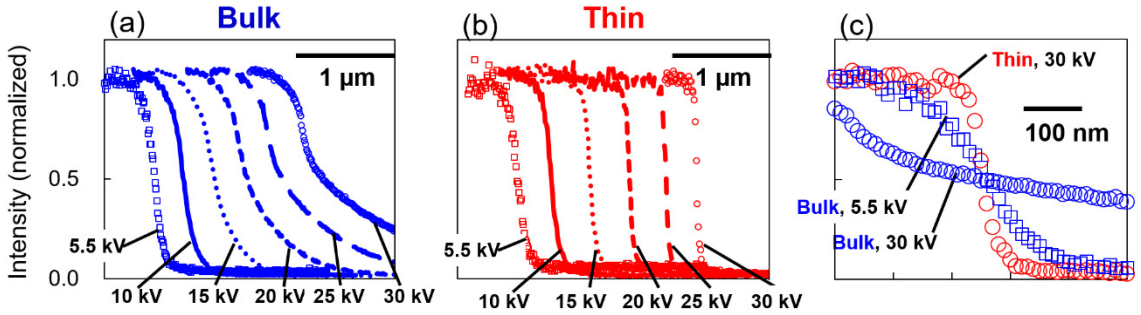

Figure 4. In-Lα line profiles across the InGaP/GaAs interface for a) bulk, and b) thin samples, obtained at V_{acc} of 5.5, 10, 15, 20, 25, and 30 kV at an I_{prob} of 50 nA. c) Results for a thin sample (V_{acc} = 30 kV), and bulk samples (V_{acc} = 30 kV and 5.5 kV). (Modified with permission from Ref. [12], copyright © 2013 Elsevier B.V. All rights reserved.)

To explain this contrast between the results for bulk and thin samples, the relationship among V_{acc}, the electron scattering area, and the SR is summarized in figure 5. The shape of the electron scattering area in the sample changes from hemispherical to droplet-shaped with an increase in V_{acc}, as depicted in the upper right panel of figure 5. This has been reported by many authors [25] and can be briefly confirmed by Monte Carlo simulation. Therefore, the lateral width of the electron scattering in the bulk sample is closely related to the SR, such that a higher V_{acc} results in a reduced SR. When working with thin samples, the SR is largely determined by the lateral size of the scattering area at the bottom of the thin film, as demonstrated in the lower right panel of figure 5. As a result, a higher V_{acc} value improves the SR. Thus, we can make the important conclusion that a high SR value is obtained when a higher V_{acc} is employed in the case of thin-sample FEG-EPMA, whereas a lower V_{acc} is necessary for bulk-sample FEG-EPMA. In addition, the use of a lower V_{acc} limits the detectable characteristic X-ray lines. Furthermore, at lower V_{acc}, the SR in thin-sample FEG-EPMA is similar to that in bulk-sample FEG-EPMA. This is because the width of the electron scattering area becomes as small as the sample thickness in thin-sample FEG-EPMA at lower V_{acc}, as shown in figure 5b.

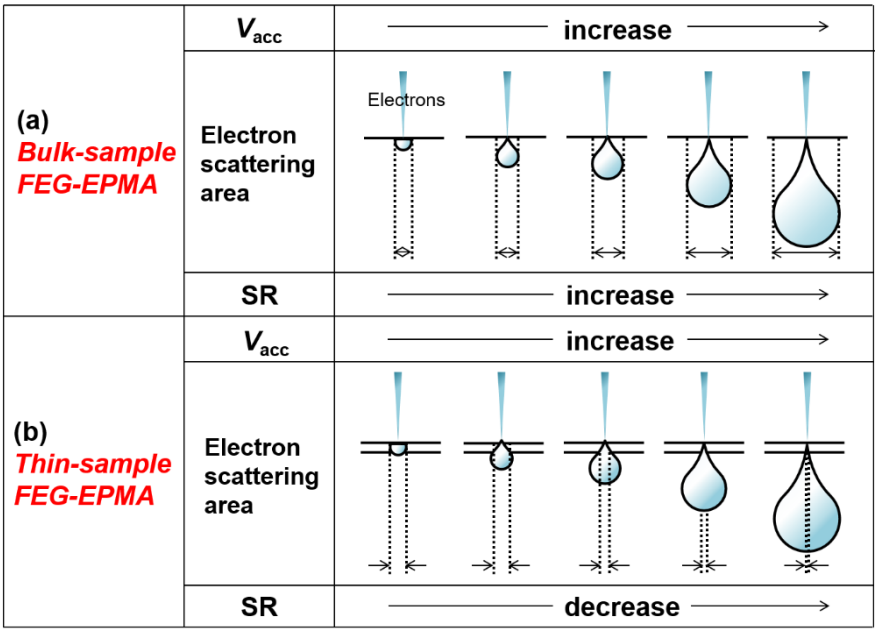

Figure 5. The V_{acc}, electron scattering area, and SR values for a) bulk- and b) thin-sample FEG-EPMA. (Modified with permission from Ref. [12], copyright © 2013 Elsevier B.V. All rights reserved.)

Figure 4c shows the line profiles for (1) a thin sample (V_{acc} = 30 kV), and (2) a bulk sample at V_{acc} = 30 and 5.5 kV. A comparison of (1) and (2) shows that the variation in the In-content across the InGaP/GaAs interface of the thin sample is significantly sharper than that in the bulk samples, which demonstrates enhancement of the FEG-EPMA SR as a result of sample thinning. In bulk-sample FEG-EPMA, the use of a lower V_{acc} enables higher resolution analyses; however, even bulk-sample FEG-EPMA at V_{acc} = 5.5 kV is inferior to thin-sample FE-EPMA at 30 kV in terms of the SR, as evident from a comparison of (1) and (3).

3.2. SR and MDL values for bulk- and thin-sample FEG-EPMA

Figure 6 summarizes the relationships between the SR and MDL for bulk- and thin-sample FEG-EPMA and STEM-EDS analyses of In within the InGaP layer of InGaP/GaAs samples. Based on the discussion in Section 3.1, V_{acc} was set to 30 kV for thin-sample FEG-EPMA in conjunction with T values of 100, 130, 210, 310, and 430 nm, while V_{acc} was 5.5 or 10 kV for bulk-sample FEG-EPMA. In all cases, I_{prob} values of 5, 20, 50, 100, or 200 nA were used. The results presented in figure 4

indicate that thin-sample FEG-EPMA simultaneously results in better SR and higher sensitivity, i.e., a lower MDL, compared to bulk-sample FEG-EPMA and STEM-EDS. The SR values obtained from thin-sample FEG-EPMA range from 40 to 350 nm and the MDL values from 13,000 to 600 ppm under the present measurement conditions. In addition, it is evident that both the SR and MDL can be tuned by varying T, and that T should be less than approximately 300 nm, because the advantages of thin-sample FEG-EPMA are lost as the samples become thicker. The SR and MDL values required for EDF analysis (50 nm and 5,000 ppm) are indicated by the region labelled "Requirements" in figure 6. Thin-sample FEG-EPMA partly met these requirements, while bulk-sample FEG-EPMA and STEM-EDS did not with an I_{prob} of 50 - 100 nA and T of 100 nm. Here we also note that it is important to consider the difference in density between InGaP/GaAs and impurity-doped SiO_2, and that the SR in the SiO_2 can be estimated via a Monte Carlo simulation in conjunction with the measured SR for InGaP/GaAs [12-14]. In Ref. [13], the SR was estimated and the MDL was measured for trace Cl-doped SiO_2 thinned to 140 nm. The SR values of Cl were 31, 33, 41, 55, and 113 nm for I_{prob} of 5, 20, 50, 100, and 200 nA, whereas the MDL values were 655, 491, 446, 392, and 224 ppm (by mass), respectively. These combinations of SR and MDL are plotted as "Thin-sample FEG-EPMA (Cl-doped SiO_2)" in figure 6.

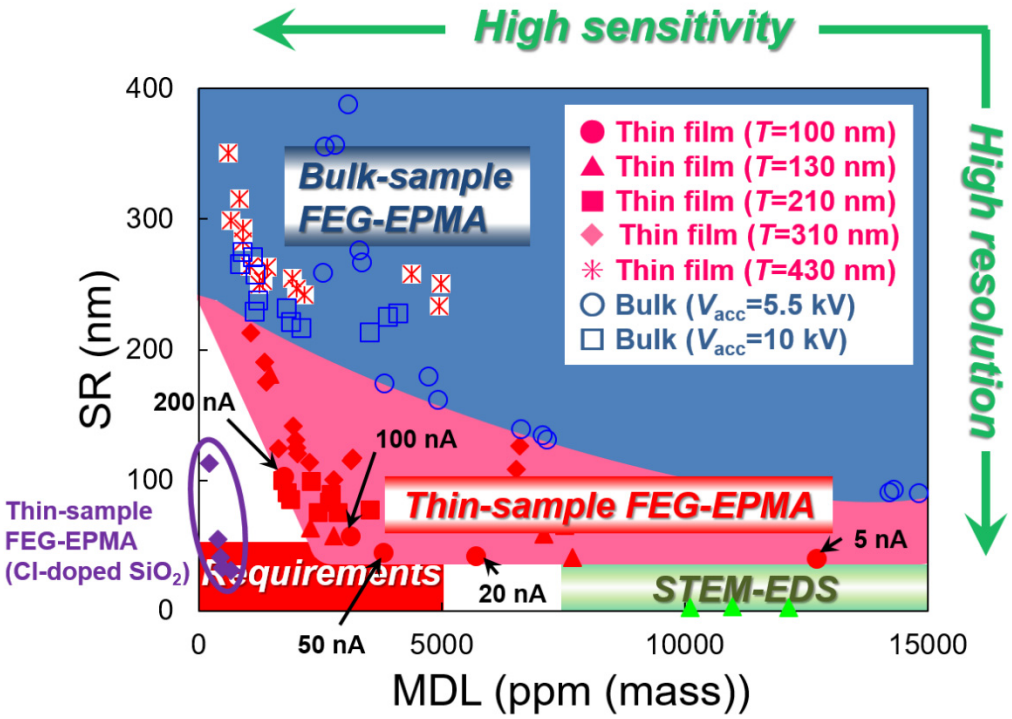

Figure 6. Relationships between SR and MDL for thin- and bulk-sample FEG-EPMA along with that for STEM-EDS. For thin-sample FEG-EPMA, V_{acc} was set to 30 kV and the T value ranged from 100 to 430 nm. For bulk-sample FEG-EPMA, V_{acc} was set to 5.5 or 10 kV. I_{prob} values were set to 5, 20, 50, 100, and 200 nA. For thin film (T = 100 nm), the I_{prob} indications were added in the figure. These data show that thin-sample FEG-EPMA allows combinations of SR and MDL that bulk-sample EPMA and STEM-EDS do not. (Modified with permission from Ref. [13], copyright © 2015 Elsevier B.V. All rights reserved.)

3.3. Variation of SR and MDL with T

At this point, we discuss two issues connected with thin-sample FEG-EPMA: the reason why a high SR can be obtained without significant degradation of the MDL and why the advantages of this method are not evident for samples thicker than 300 nm. The white circles, triangles, and squares in figure 7a show the relationship between T and the measured SR values for thin-sample FEG-EPMA (V_{acc} = 30 kV, I_{prob} = 5 - 50 nA). Monte Carlo simulations were also performed to examine the validity of the experimental SR values, as follows [13]. The SR is mainly determined by the sum of the diameter of the electron beam on the sample surface and the lateral width of the X-ray generation region in the sample [11]. We first calculated the lateral width of the area containing 70 % of the number of collisions between incident electrons and atomic electrons using Monte Carlo simulation for sample thicknesses of 100, 130, 210, 310, and 430 nm. Here, these calculated lateral widths are defined as R. For the sample thickness of 100 nm, the beam diameter on the sample surface was determined such that the sum of the beam diameter and the calculated R was equal to the measured SR. The beam diameter on the sample surface was determined to be independent of the sample thickness. In figure 7a, we show the sum of R for the respective sample thicknesses and the beam diameters together with the measured SR as solid circles, triangles, and squares. These data indicate that these sums are larger than the measured SR in the case of thicker samples. We attribute this result to the smaller lateral width of the characteristic X-ray generation area compared with that of the electron scattering area. In addition, both the measured and simulated SRs exhibit approximately linear correlations with T up to 210 nm, although this correlation drops off at 310 nm.

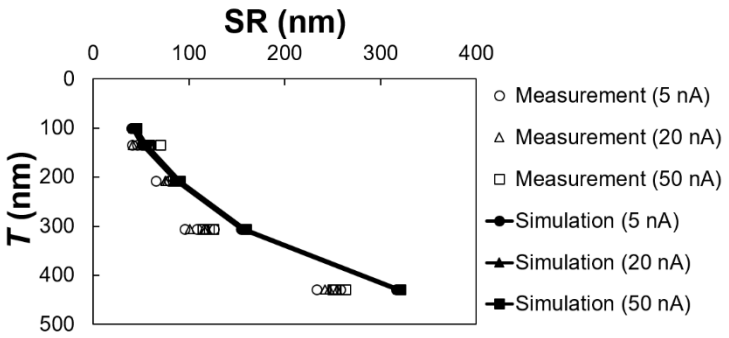

Figure 7. Relationship between T and SR for thin-sample FEG-EPMA. (Modified with permission from Ref. [13], copyright © 2015 Elsevier B.V. All rights reserved.)

To better explain these findings, figure 8 presents diagrams of the electron scattering regions in bulk and thin samples. The scattering area is droplet-like in the bulk sample, as depicted in figure 2. At depths below approximately 300 nm, the lateral width of the scattering area increases. For thin-sample FEG-EPMA, the lateral size of the scattering area at the bottom of the thin sample primarily determines the SR. Therefore, the degradation in SR with increasing T exceeds that expected from a linear relationship at large T (figure 8b).

Figure 9a plots the linear relationship between the X-ray intensity and T for I_{prob} values of 5 to 200 nA, based on the average In-Lα X-ray intensity along the line profile in the InGaP layer. Nomura *et al*. previously reported the relationship between V_{acc} and X-ray intensity for thin-sample FE-SEM-EDS analysis with various T [26]. A close examination of their plots reveals that the X-ray intensity was proportional to T, although this was not specifically identified by the authors. In the present study, figure 9b plots the relationship between the MDL and the reciprocal of the square root of the X-ray intensity for different combinations of T and I_{prob}. The data can be well fitted using the linear function y = 137836x + 172.89, i.e., the MDL is approximately proportional to the reciprocal of the square root of the X-ray intensity [27]. Considering the results in both figures 9a and 9b, it can be concluded that the MDL is also proportional to the reciprocal of the square root of T. The results of

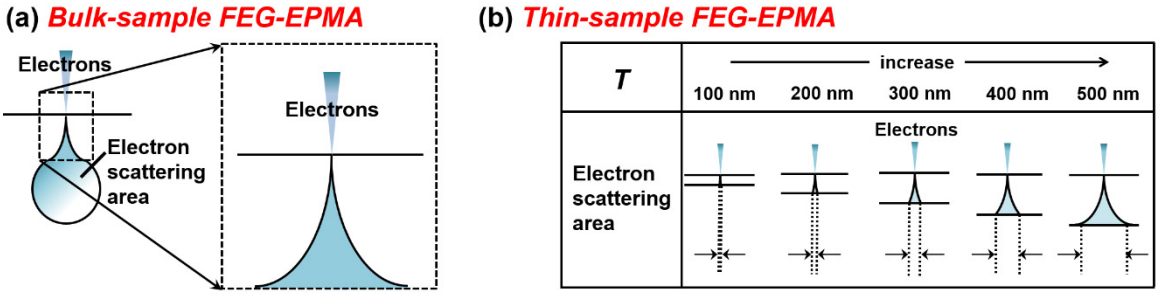

Figure 8. Schematic diagrams of the electron scattering areas for bulk- and thin-sample FEG-EPMA. a) Droplet-like scattering area for bulk-sample FEG-EPMA. b) Electron scattering area for thin-sample FEG-EPMA, which varies with *T*. At depths greater than approximately 300 nm, the lateral width of the scattering area increases more strongly. In the case of thin-sample FEG-EPMA, SR is largely determined by the lateral width of the scattering area at the bottom of the thin sample. Therefore, the degradation in SR with increasing T exceeds that predicted by a linear relationship. (Modified with permission from Ref. [13], copyright © 2015 Elsevier B.V. All rights reserved.)

this detailed investigation into the effect of *T* on the SR and MDL lead to several conclusions. Firstly, the SR value exhibits a linear dependence on *T*, whereas the MDL is inversely proportional to the square root of *T*. Therefore, thinning of a sample for FEG-EPMA allows the SR to be improved without any significant degradation of the MDL. In addition, the lateral width of the scattering area increases at depths greater than about 300 nm, such that an increase in *T* beyond 300 nm significantly reduces the SR without any appreciable degradation of the MDL. Based on the first point, thinning of the sample to less than 100 nm would be expected to significantly improve the SR without a significant increase in the MDL. However, reproducible fabrication of samples thinner than 100 nm is difficult, and raises concerns regarding sample deformation and non-uniform *T*. Furthermore, any damage to the sample is likely to have an effect on the FEG-EPMA measurement results for very thin samples.

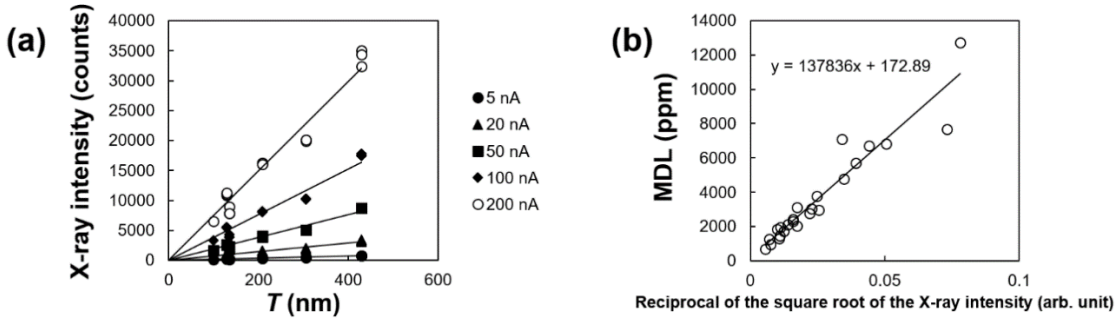

Figure 9. Relationship between a) X-ray intensity and *T* for thin-sample FEG-EPMA, and b) MDL as a function of the reciprocal of the square root of the X-ray intensity for various *T* and I_{prob}. (Modified with permission from Ref. [13], copyright © 2015 Elsevier B.V. All rights reserved.)

3.4. Thin-sample FEG-EPMA of EDF

Figure 10 shows line profiles obtained using a) bulk- and b) thin-sample FEG-EPMA around the EDF core, along with diagrams depicting the correlation between the size of the electron scattering area and the actual elemental distribution around the EDF core. Reductions at the centre of the core are clearly evident for both the Al and Ge intensities. The details of the sample preparation procedure and measurement conditions for the analysis of the EDF core are described in Ref. [14]. Prior to the FEG-EPMA measurements, the EDF samples were assessed using STEM-EDS to determine the distribution of dopants obtained via conventional microsampling. However, our experimental work demonstrates that the analysis of an EDF using conventional STEM-EDS is difficult due to both insufficient MDL values and potential sample damage [14].

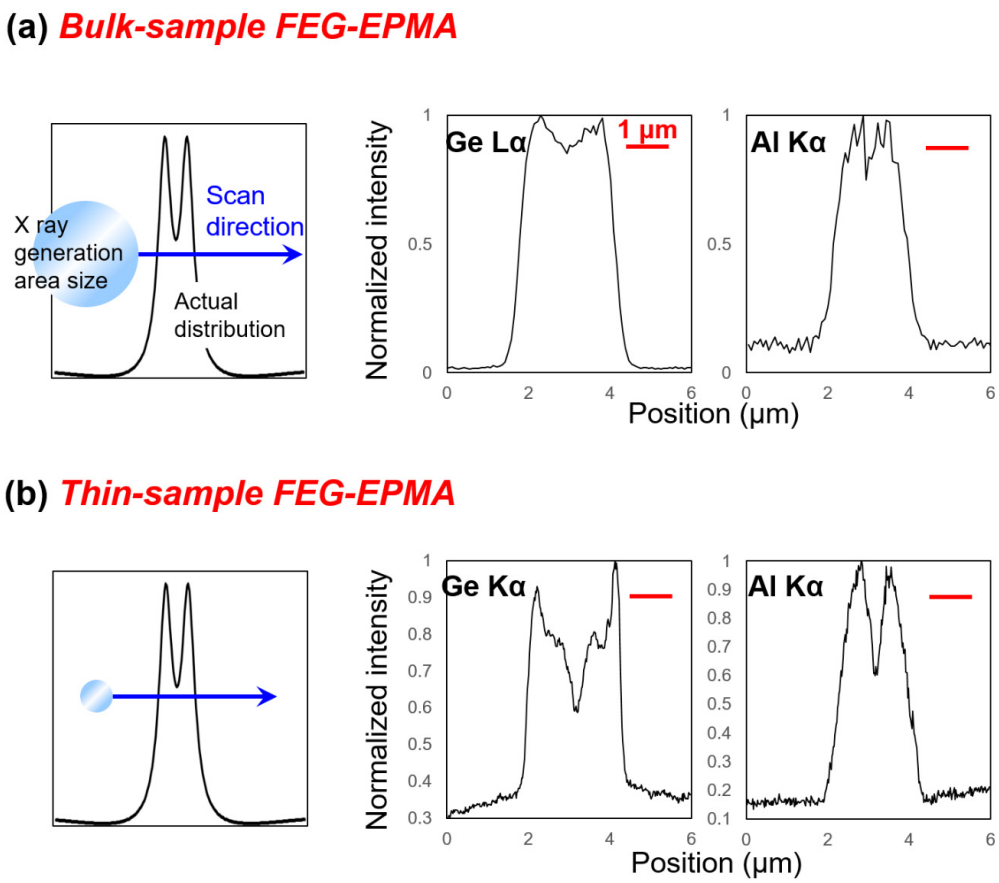

Figure 10. Comparison of line profiles for a) bulk-, and b) thin-sample FEG-EPMA analysis around the EDF core containing Er. The Y-axis is the X-ray intensity normalised with respect to the maximum. (Modified with permission from Ref. [14], copyright © Microscopy Society of America 2015.)

Finally, another advantage of thin-sample FEG-EPMA is discussed along with two important associated issues that require further thorough study. This additional advantage is related to the X-ray lines that are employed in the analysis. One of the most serious challenges in bulk-sample FEG-EPMA is the use of low V_{acc} during high resolution analyses, because a low V_{acc} can adversely affect the accuracy of quantitative work. When operating FEG-EPMA instrumentation at low V_{acc}, it

is typical to use low-energy X-ray lines such as the L- or M-lines. In addition, the fluorescence yields for the L- and M-lines are lower than those for the conventional K-line. In contrast, the thin-sample FEG-EPMA technique described herein employs high V_{acc} that enhances the SR. As a result, it is possible to use high-energy X-ray lines for data quantification [9].

The first issue for further consideration is the potential for electron beam damage during the analysis of insulating samples [12]. Under typical measurement conditions, the doses applied in FEG-EPMA are lower than those used during STEM-EDS. The electron probe doses at the sample surface were calculated for both FEG-EPMA and STEM-EDS analysis and were estimated to be 6.37×10^5 C/cm^2 (STEM), 7.08×10^4 C/cm^2 (EPMA, I_{prob} = 5 nA) and 7.08×10^3 C/cm^2 (EPMA, I_{prob} = 200 nA), assuming respective probe sizes of 0.2, 3 and 60 nm. On the basis of these simple estimations, it can be assumed that (1) sample damage due to electron beam radiation will be considerably smaller in the case of FEG-EPMA than for STEM-EDS based on the relative doses, and (2) a larger I_{prob} results in less sample damage during FEG-EPMA. Nevertheless, electron beam damage can become a serious problem because much higher V_{acc} and I_{prob} are required to maximise the advantages of thin-sample FEG-EPMA. In our previous experiments [14], application of V_{acc} at 30 kV and I_{prob} at 200 nA resulted in serious plastic deformation of the sample due to a local rise in temperature by electron beam irradiation. Therefore, it is apparent that novel sample preparation techniques will be required to limit sample damage during thin-sample FE-EPMA. We have reported one such technique in a previous paper [14], applied to the analysis of the EDF core described in this review.

The second challenge is related to the development of methods to use thin samples for quantitative analysis, just as techniques for the quantitative microanalysis of EDS and WDS samples have been widely researched for several decades [28, 29]. In the case of thin-sample FEG-EPMA, the quantification techniques used for bulk samples cannot be directly transferred, because the matrix effect is dependent on T, as with the chemical composition. If calibration standards can be prepared with the same T as the sample to be analysed, then quantitative analysis can be readily performed, otherwise such analysis is difficult. Despite these two challenges, we consider that thin-sample FEG-EPMA is a very promising technique for the analysis of various materials because these two issues have been addressed in a number of individual laboratory studies.

It should be noted that we have omitted the contributions of Monte Carlo simulations to this field of research in the present review for reasons of space. However, such simulations were performed to a significant extent and were found to be extremely helpful to confirm the validity of the experimental results. The interested reader is referred to our previous reports [13, 14] for details of these simulations.

4. Conclusions

This mini-review described the SR and MDL values obtained when employing FEG-EPMA. InGaP samples were thinned to approximately 100, 130, 210, 310, and 430 nm to allow for effective thin-sample FEG-EPMA in the resolution range of 40 - 350 nm and the MDL range of 13,000 - 600 ppm (by mass). It is clear that thin-sample FEG-EPMA can achieve both lower MDL and better SR values than are possible with bulk-sample FEG-EPMA or STEM-EDS. This is because the majority of the X-rays that determine the MDL are generated in the surface region of the sample to depths of about 300 nm during FEG-EPMA. The SR and MDL can also be tuned by variation of the I_{prob} and T in accordance with the analytical purpose. Finally, thin-sample FEG–EPMA was applied to the analysis of dopant distributions in an EDF core. Using this technique, the Al and Ge distributions in an EDF could be observed. Thus, the present technique is suitable as a laboratory technique for microstructural analysis.

Acknowledgements
The author wishes to thank the following individuals for fruitful discussions: Prof. J. Fujita and Prof. T. Kizuka of the University of Tsukuba, Dr. H. Takahashi and Mr. N. Mori of JEOL, Ltd., and Mr. K. Hamada, Dr. K. Yamaguchi, Dr. J. Iihara and Mr. S. Matsukawa of Sumitomo Electric Industries, Ltd. The author also thanks the following individuals for technical support during this work: Mr. K. Sugawara of the Foundation for the Promotion of Material Science and Technology of Japan, and Dr. K. Kuramochi, Mr. T. Haruna, Mr. K. Sasaki, and Mr. K. Hase of Sumitomo Electric Industries, Ltd.

References
[1] Rinaldi R and Llovet X 2015 *Microsc. Microanal.* **21** 1053
[2] Kimura T, Nishida K and Tanuma S 2006 *Mikrochim. Acta* **155** 175
[3] Berger D and Nissen J 2014 *IOP. Conf. Ser.: Mater. Sci. Engng.* **55** 012002
[4] McSwiggen P 2014 *IOP Conf. Ser.: Mater. Sci. Engng.* **55** 012009
[5] Pinard P T and Richter S 2014 *IOP Conf. Ser.: Mater. Sci. Engng.* **55** 012016
[6] Fournelle J, Cathey H, Pinard P T and Richter S 2016 *IOP Conf. Ser.: Mater. Sci. Engng.* **109** 012003
[7] Kubo Y and Yonezawa K 2017 *Anal. Chem.* **89** 8772
[8] Haruna T, Iihara J, Yamaguchi K, Saito Y, Ishikawa S, Ohnishi M and Murata T 2006 *Opt. Express* **14** 11036
[9] Merlet C and Llovet X 2012 *IOP Conf. Ser.: Mater. Sci. Engng.* **32** 012016
[10] Lorimer G W, Cliff G and Clark J N 1975 in: *Developments in electron microscopy and analysis. EMAG 75*. (Venables J A ; ed.) (London: Academic Press) 153
[11] Goldstein J I, Costley J L, Lorimer G W and Reed S J B 1977 *Proc. of the Workshop on Analytical Electron Microscopy, SEM 1977, v*ol. 1 (Chicago: IIT Research Institute) 315
[12] Kubo Y, Hamada K and Urano A 2013 *Ultramicroscopy* **135** 64
[13] Kubo Y and Hamada K 2015 *Ultramicroscopy* **157** 48
[14] Kubo Y and Kuramochi K 2015 *Microsc. Microanal.* **21** 1398
[15] Champness P E, Cliff G and Lorimer G W 1982 *Ultramicroscopy* **8** 121
[16] Joy D C and Maher D M 1977 *Proc. of the Workshop on Analytical Electron Microscopy, SEM 1977,* vol. 1. (Chicago: IIT Research Institute) 325
[17] Horita Z, Sano T and Nemoto M 1987 *Ultramicroscopy* **21** 271
[18] Watanabe M and Williams D B 1999 *Ultramicroscopy* **78** 89
[19] Richter S, Bückins M, Aretz A, Kyrsta S, Spähn M and Mayer J 2004 *Microchim. Acta* **145** 187
[20] Richter S, Kyrsta S, Schneider J, Hajas D and Mayer J 2006 *Microchim. Acta* **155** 257
[21] Richter S and Pinard P T 2016 *IOP. Conf. Ser.: Mater. Sci. Engng.* **109** 012014
[22] Barkshire I, Karduck P, Rehbach W P and Richter S 2000 *Mikrochim. Acta* **132** 113
[23] Japanese Industrial Standards Committee 2012 JIS K0114:2012, General Rules for Gas Chromatography (Tokyo: Japanese Standards Association)
[24] French W G, Pearson A D, Tasker G W and Macchesney J B 1973 *Appl. Phys. Lett.* **23** 338
[25] For example, Duncumb P and Shields P K 1963 *Br. J. Appl. Phys.* **14** 617
[26] Nomura S, Todokoro H and Komada T 1975 in: *Scanning electron microscopy 1*. (Johari O and Corvin I; eds.) (Chicago: IIT Research Institute) 103
[27] Jenkins R, Gould R W and Gedcke D 1981 *Quantitative X-ray spectrometry*. (New York: Marcel Dekker, Inc.)
[28] Cliff G and Lolimer G W 1975 *J. Microsc.* **103** 203
[29] Watanabe M and Williams D B 2006 *J. Microsc.* **221** 89